Fundamental Study on Vertical and Longitudinal Force Control for Electric Airplane with Multiple Propellers

Tokuma Ikegami[*a)] Student Member, Hiroshi Fujimoto[*] Senior Member
Akira Nishizawa[**] Non-member, Hiroshi Kobayashi[**] Non-member
Yasumasa Watanabe[*] Non-member

Aircrafts are desired to be more energetically efficient and safer due to the increasing demand of air transportations. Generally, business airplanes tend to have low stability under wind disturbances especially during landing. Due to electric motor's high performances among motion control compared to internal combustion engines, electric airplanes, in which electric motors are used for propulsion, can satisfy the demands of both efficiency and safety. In this paper, by utilizing electric motors' advantages, lift control method using propeller slipstream as well as thrust control is proposed. The effectiveness of the proposed method is verified by simulations.

Keywords: Electric Airplane, Lift control, Thrust control, Propeller, Slipstream, Motor

1. Introduction

1.1 Background Recently, due to global warming and oil price pumping, hybrid electric vehicles (HEVs) and electric vehicles (EVs) have been wildly developed among the automobile industry. Due to the increasing demands of air transportation, aircrafts are also desired to be more energy efficient [(1) (2)].

Electric airplanes (EAs) are believed to be a solution towards these problems by the utilization of electric motors for propulsion [(3) (4)]. Apart from the environmental benefit, motors have the following remarkable advantages compared with internal combustion engines (ICEs).

- Response of motor torque is much faster than that of ICEs.
- Distributed installation and independent control are easy.
- Motor torque can be measured precisely from motor current.

Furthermore, as the technological exchange between the automotive and the aviation industry have been very active, the highly developed motion control theories in the automotive industry can be adapted to airplanes.

There are some studies on safety and efficiency control for EAs by utilizing these advantages, among some of which EAs with multiple motors and propellers are selected [(5) (6)].

1.2 Objective Including EAs, present airplanes are designed to give higher stability and controllability. The thrust and the lift are the essential factors that must be controlled, in order to prevent accident during approaching and landing.

However, landing weight of EAs are larger than that of conventional internal combustion airplanes, because that the weight of the battery-powered EAs does not change through flight while the fuel-powered conventional plane become lighter as oil have been combusted.

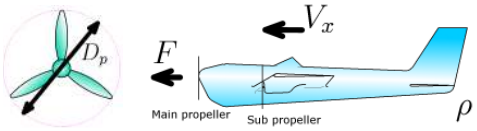

(a) Propeller diameter. (b) Thrust and wind speed, air density.

Fig. 1. Definitions of the parameters.

We have proposed a lift control system adapting the slipstream of propellers on the wing [(6)]. However, this control method does not include thrust control which can cause fatal accident when the airplane received back wind. Furthermore, the control system creates an ineligible thrust change while actively changing the revolution speed of the propellers on the wing, causing a fatal acceleration while landing. In order to solve the problem, this paper proposes a vertical and longitudinal force concurrency control method using independent control of motor torque to of propellers on the nose and the wing. The proposed method can be applied to an airplane that has three propellers. In the future, the proposed system will be needed for a vertical and longitudinal velocity control.

2. Modeling

To design the lift and thrust concurrency control system, the plant model should be discussed. First, the model of propeller and its slipstream are explained by using fluid dynamics. Second, the model of lift caused by slipstream is also explained by using slipstream model.

2.1 Propeller aerodynamics V_x and ρ are defined as

a) Correspondence to: ikegami15@hflab.k.u-tokyo.ac.jp
* The University of Tokyo
5-1-5, Kashiwanoha, Kashiwa-shi, Chiba, Japan, 277-8561
** Japan Aerospace Exploration Agency
6-13-1, Osawa, Mitaka-shi, Tokyo, Japan, 181-0015

© 2016 The Institute of Electrical Engineers of Japan.

airplane longitudinal velocity and air density. D_p is defined as propeller diameter as shown in Fig. 1(a). n is defined as propeller revolution speed. Advance ratio J is defined by Eq. (1).

$$J = \frac{V_x}{nD_p}. \tag{1}$$

Then, thrust F generated by propeller revolution and counter torque Q can be calculated by Eq. (2),(3).

$$F = C_F(J)\rho n^2 D_p^4, \tag{2}$$
$$Q = C_Q(J)\rho n^2 D_p^5, \tag{3}$$

where, $C_F(J)$ and $C_Q(J)$ are non-dimensional coefficient of thrust F and counter torque Q. Generally, both of them is a function of J. J is a function of n, so $C_F(J)$ is also a function of n.

2.2 Modeling of propeller slipstream speed When a propeller rotates and creates thrust, propeller slipstream is amplified with an increase of airspeed. The aerodynamics of propeller slipstream is studied [7] [8]. In this part, the model of propeller slipstream is introduced.

V_p is defined as wind speed the crossing rotational surface of propeller and V_s is defined as the wind speed of the propeller slipstream. P_∞ is defined as the atmospheric pressure, P_f is defined as the pressure at the front of the propeller, and P_r is defined as the pressure of the rear of the propeller.

Eq. (4) and Eq. (5) are calculated by the Bernoulli's principle. Eq. (4) shows the balance of the infinite distance ahead to the front face of the propeller, and Eq. (5) shows the balance of the rear face of the propeller to the infinite distance of behind.

$$\frac{1}{2}\rho V_x^2 + P_\infty = \frac{1}{2}\rho V_p^2 + P_f, \tag{4}$$
$$\frac{1}{2}\rho V_p^2 + P_r = \frac{1}{2}\rho V_s^2 + P_\infty. \tag{5}$$

Thrust can be interpreted as the force on the propeller caused by the air pressure difference between the front and the rear face of the propeller. Eq. (6) is obtained as propeller thrust can be calculated by multiplying the disk-area of the propeller to the pressure difference.

$$F = \frac{1}{4}\pi D_p^2 (P_r - P_f). \tag{6}$$

Eq. (7) can be obtained by Eq. (4)–(6).

$$F = \frac{\pi}{8}\rho V_x^2 D_p^2 \left\{ \left(\frac{V_s}{V_x} \right)^2 - 1 \right\}. \tag{7}$$

Then, the model of propeller slipstream can be rewritten as [6]

$$V_s = V_x \sqrt{1 + \frac{8}{\pi} C_F(J) J^{-2}}. \tag{8}$$

2.3 Modeling of wing aerodynamics In this paper, it is assumed that an airplane is equipped with three propellers: two bigger sub-propellers on both wings and a smaller main-propeller on the nose shown in Fig. 2.

S_w is defined as the total main wing area, and S_p is defined as the wing area affected by a single propeller's slipstream while S_n is defined as the wing area not affected by propeller slipstream. Thus, the equation below holds

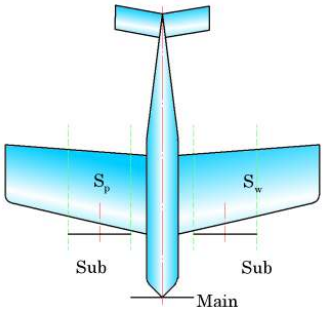

Fig. 2. Position of main and sub-propeller.

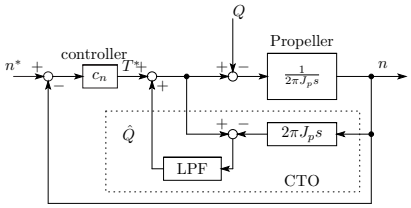

Fig. 3. Propeller revolution speed control system.

$$S_w = 2S_p + S_n. \tag{9}$$

C_L and C_D is respectively lift and drag coefficient determined by the airfoil of the wing or angle of attack. Total lift L_{all} is the summation of the lift L_{prop} created by the S_p area. The lift L_n created by the S_n area as Eq. (10).

In the same way, the total drag D_{all} is a summation of drag D_{prop} created by the S_p area and drag D_n by created by the S_n area as Eq.(11).

$$\begin{aligned} L_{all} &= L_n + 2L_{prop} \\ &= \frac{1}{2}\rho C_L S_n V_x^2 + \frac{1}{2}\rho C_L S_p V_s^2, \end{aligned} \tag{10}$$
$$\begin{aligned} D_{all} &= D_n + 2D_{prop} \\ &= \frac{1}{2}\rho C_D S_n V_x^2 + \frac{1}{2}\rho C_D S_p V_s^2. \end{aligned} \tag{11}$$

3. Controller design

In this part, lift and thrust concurrency control is proposed. The proposed method needs high-performance propeller revolution speed control system. First, the revolution speed controller including counter torque observer (CTO) is explained. Second, multi-input multi-output (MIMO) system for lift and thrust is proposed based on the characteristics experiment. Finally, the controllers of MIMO system is designed.

3.1 Revolution speed controller Equation of propeller motion is expressed as

$$2\pi J_p \dot{n} = T - Q. \tag{12}$$

where J_p is defined as the inertia of the propeller. If motor torque T and revolution speed n are measurable, counter torque Q of the propeller can be estimated by disturbance observer named the propeller counter torque observer. By using that, the plant is nominalized as Eq. (13) at frequency ranges below the cut-off frequency ω_g of the low pass filter (LPF)

$$P_{nom} = \frac{1}{2\pi J_p s}. \tag{13}$$

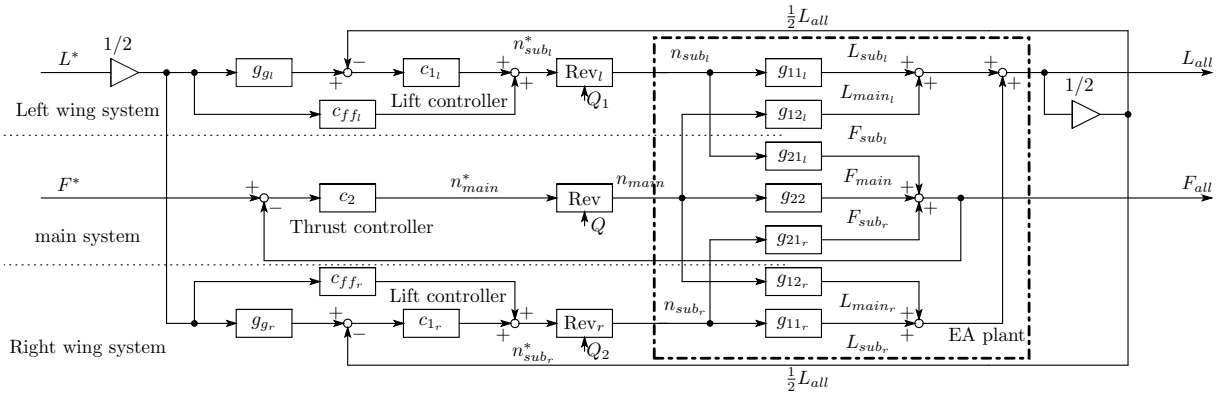

Fig. 4. Lift control with thrust control system.

The revolution speed controller is designed by proportional controller c_n shown in Fig. 3. The gain of c_n is decided by pole placing at ω_n. Then, the transfer function from revolution speed reference n^* to revolution speed n is expressed as Eq. (14).

$$G_n = \frac{n}{n^*} = \frac{\omega_n}{s + \omega_n}. \tag{14}$$

Here, the gain c_n is calculated by Eq. (15).

$$c_n = 2\pi J_p \omega_n. \tag{15}$$

3.2 MIMO system In this paper, the object is simultaneous control of thrust and lift by the propeller. Therefore, a multi-input multi-output system is proposed (Fig. 4) due to two target values for simulation thrust and lift.

The accent $*$ means the reference input. The subscripts r/l means left/right. The blocks $c_{g_{r/l}}$ are reference models for feedforward controller. The blocks $c_{ff_{r/l}}$ is the feedforward controller, The blocks $c_{1_{r/l}}$ and c_2 are the feedback controllers. The Rev blocks in Fig. 4 are revolution speed control system shown in Fig. 3. The blocks $g_{11_{r/l}}$ are the transfer functions from the revolution speed of sub-propeller to the lift caused by slipstream. The blocks $g_{21_{r/l}}$ are the transfer functions from sub-propeller to the thrust. The block g_{22} is the transfer functions from main-propeller to the thrust. Finally, the blocks $g_{12_{r/l}}$ are the transfer function from main-propeller to the lift.

The slipstream of main-propeller interfere to the lift. Interference of main-propeller is experimented using wind tunnel shown in Fig. 5. The propeller APC 10×10 is used for the sub-propeller and APC 7×10 is used for the main-propeller in this experiment. The main-propeller is fixed at in front of airplane model in the wind tunnel and changed the revolution speed reference like Fig. 6(a). The sub-propeller is fixed at the left wing of airplane model in the wind tunnel and changed the revolution speed reference like Fig. 6(b). The wind speed set at 10 m/s and the angle of attack of the airplane set at 7 deg. The variation of the lift is measured.

The characteristics experimental result shown in Fig. 6. In this experiment, the sub-propeller is fixed at only the left wing. When 2 sub-propellers are fixed at both wing, the variation of the lift from 0 rpm revolution speed should be twice bigger than what the Fig. 6 has show. Thus, the change of lift caused by the slipstream of the main-propeller is much small than that of the main wings (as shown in Fig. 6(c)). As a result the lift caused by the main-propeller's slipstream can be

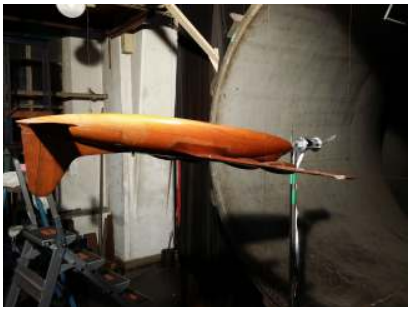

Fig. 5. Experimental instruments.

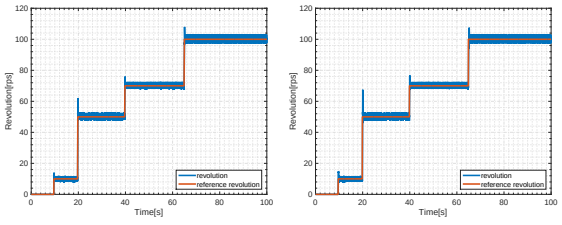

(a) Revolution of main-propeller. (b) Revolution of left-propeller.

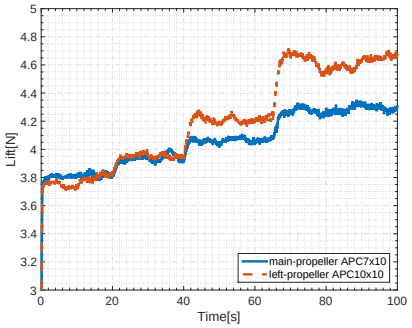

(c) Lift variation caused by main-propeller and sub-propeller.

Fig. 6. Interference by main-propeller.

neglected and g_{12} can be put as 0 ($g_{12} = 0$).

3.3 Lift controller and thrust controller Lift controller consists of a integrated feedback controller and the feedforward controller. The propeller performance has been researched for years [9]~[14], however the propeller analysis

model is not available. In this paper, the propeller model is built by linearization using experimental data. C_F can be quadratically approximated using experimental data as Eq.(16) [5].

$$C_F(J) \simeq a_{C_F} J^2 + b_{C_F} J + c_{C_F}. \tag{16}$$

Then, Eq. (17) is derived from by Eq. (8), Eq. (10) and Eq. (16).

$$L_{prop} \simeq \alpha_L n^2 + \beta_L n + \gamma_L, \tag{17}$$

where,

$$\alpha_L = \frac{4}{\pi} C_L \rho S_s c_{C_F} D_p^2,$$
$$\beta_L = \frac{4}{\pi} C_L \rho S_s D_p b_{C_F} V_x,$$
$$\gamma_L = \frac{1}{2} C_L \rho S_s \left(\frac{8}{\pi} a_{C_F} + 1 \right) V_x^2.$$

Eq. (17) is defined as function $f_{L_s}(n) = \alpha_L n^2 + \beta_L n + \gamma_L$. Eq. (18) can be obtained from Taylor expansion of Eq. (17) at n_{nom} for linearization.

$$f_{L_s}(n) \simeq (2\alpha_L n_{nom} + \beta_L) n + \alpha_L n_{nom}^2 + \beta_L n_{nom} + \gamma_L. \tag{18}$$

From Eq. (1) and Eq. (16), Eq. (2) is approximated to Eq. (19). And Eq. (19) is defined as function $f_F(n) = \alpha_F n^2 + \beta_F n + \gamma_F$.

$$F \simeq \alpha_F n^2 + \beta_F n + \gamma_F, \tag{19}$$

where,

$$\alpha_F = \rho c_{C_F} D_p^4,$$
$$\beta_F = \rho b_{C_F} D_p^3 V_x,$$
$$\gamma_F = \rho a_{C_F} D_p^2 V_x^2.$$

Using $f_F(n)$, g_{21} and g_{22} are approximated as Eq. (21) and Eq. (22).

$$g_{11} \simeq f_{L_s}(n_s), \tag{20}$$
$$g_{21} \simeq f_{F_{sub}}(n_s), \tag{21}$$
$$g_{22} \simeq f_{F_{main}}(n_m). \tag{22}$$

The controller c_1 for the lift in Fig. 4 is designed as Eq. (23) placing the pole at ω_L.

$$c_1 = \frac{\omega_L}{s(2\alpha_L n_0 + \beta_L)}. \tag{23}$$

Due to the delay of the system, feedforward controller needs reference model g_g designed as Eq. (24).

$$g_g = \frac{\omega_g}{s + \omega_g}. \tag{24}$$

From Eq. (20) – Eq. (22), the equation of the MIMO system can be expressed as Eq. (25).

$$\begin{cases} L_{all} = L_n + 2 f_{L_s}(G_n \cdot n_{sub}^*) \\ F_{all} = f_{F_{sub}}(G_n \cdot n_{sub}^*) + f_{F_{main}}(G_n \cdot n_{main}^*) \end{cases} \tag{25}$$

Then, the feedforward controller c_{ff} is designed as Eq. (26) using reference model Eq. (24).

$$c_{ff} = \frac{g_g}{G_n} \cdot f_{L_s}^{-1}(L_s). \tag{26}$$

Supposing the convergence of the revolution speed controller is fast enough, the transfer function from n^* to n can be regarded as 1.The constant term $\alpha_L n_{nom}^2 + \beta_L n_{nom} + \gamma_L$ is canceled out by the feedback controller.

Table 1. Poles of pole placement.

pole	value
ω_{CTO}	200
ω_n	100
ω_g	20
ω_L	20

Table 2. Parameter of airplane and propeller [6].

parameter	value	dimension
ρ	1.23	kg/m^3
S_w	0.440	m^2
C_L	0.58	-
D_p of main-propeller	0.178	m
D_p of sub-propeller	0.254	m
J_p of main-propeller	0.000156	kg·m^2
J_p of sub-propeller	0.000213	kg·m^2

4. Simulation

In this part, the simulation of proposed method has been done by using MATLAB/simulink. Two kinds of simulation have been done to verify the effectiveness of the proposed control system.

- A step lift reference from 14 N to 16 N assuming the situation that a lift increase is needed during landing.
- A step thrust reference from 10 N to 11 N assuming the situation that a thrust increase is needed when hit by a tailwind.

Consider the airplane is cruising at airspeed 7 m/s. The poles of controllers are shown in Tb. 1. The simulation has used propeller APC 10×10 as the sub-propeller and APC 7×10 for the main-propeller. The performance of the propellers at the revolution speed 5000 rpm are shown in Fig. 7 and Fig. 8. Fig. 7(a) and Fig. 8(a) are the thrust coefficient curve and its approximation curve whose parameter is shown in Tb. 3 and Tb. 4. Fig. 7(b) and Fig. 8(b) are the counter torque coefficient curve and its approximation curve what parameter is shown in Tb. 3 and Tb. 4. The simulation parameters are shown in Tb. 2–4. In this simulation, it is supposed that the S_p is half of S_w. Here, thrust and counter torque coefficient characteristics are quadratically approximated as Eq. (16) and Eq. (27) using the experimental data shown in Fig. 7 and Fig. 8.

$$C_Q(J) = a_{C_Q} J^2 + b_{C_Q} J + c_{C_Q}. \tag{27}$$

The integral controller is designed as $c_2 = 28/s$. To compare motor and engine, the MATLAB/Simulink sample file sldemo_enginewc.slx is used as the engine model [16]. The input of this engine model is throttle angle, and the output is revolution speed of shaft. The gains of revolution speed controller are designed as proportional gain equal to 0.0614 and integral gain equal to 0.0723. The integral gain of lift control by engine is 5.5 and the integral gain of thrust control by engine is 5.

The simulation results are shown in Fig.9 and Fig.10. Fig. 9 shows the response of a step lift reference. Fig. 10 shows the response of a step thrust reference. Fig. 9(a), 9(b) and Fig. 10(a), 10(b) are comparing motor (red dash line) and engine (black chain line).

From Fig. 9(a), the lift is controlled and the response of motor is faster than that of engine. The thrust has kept the

Table 3. Coefficients of main-propeller.

coefficient	value
a_{C_F}	−0.0944
b_{C_F}	0.0944
c_{C_F}	0.1059
a_{C_Q}	−0.0208
b_{C_Q}	0.0307
c_{C_Q}	0.0100

Table 4. Coefficients of sub-propeller.

coefficient	value
a_{C_F}	−0.1318
b_{C_F}	0.0726
c_{C_F}	0.1126
a_{C_Q}	−0.0238
b_{C_Q}	0.0236
c_{C_Q}	0.0093

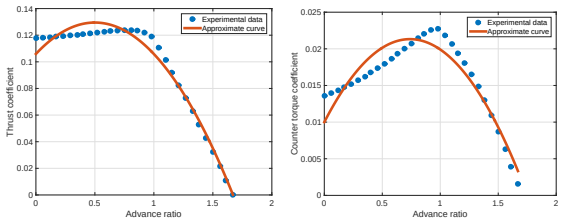

(a) Thrust coeffcient (b) Counter torque coefficient

Fig. 7. Propeller performance of APC7×10 [15]

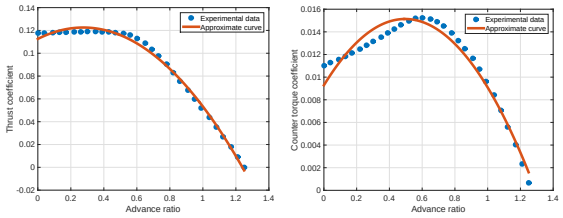

(a) Thrust coeffcient (b) Counter torque coefficient

Fig. 8. Propeller performance of APC10×10 [15]

target value by feedback. The main-propeller compensates the change of the thrust along with the change of the lift reference. In Fig. 9(b), when using the motor, thrust variation is slightly smaller than when using engine, and the time needed to converge the reference value also becomes faster than that of the engine. When the lift reference changes, the controller increases the revolution speed of sub-propeller and decreases the revolution speed of main-propeller for keeping the thrust constant shown in Fig. 9(c)–9(d).

In Fig. 10(a) and Fig. 10(b), the lift remain constant and thrust created by motor is controlled faster than that created by engine. It is shown that the main-propeller has compensated the thrust variation and kept the lift at the lift reference. When the thrust reference changes, this system increases only the revolution speed of the main-propeller for increasing the thrust keeping the lift constant as shown in Fig. 9(c)–Fig. 9(d).

From the above, the effectiveness of proposed method is

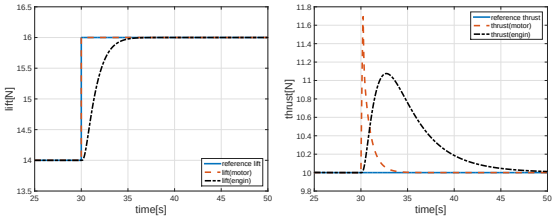

(a) Response of lift. (b) Response of thrust.

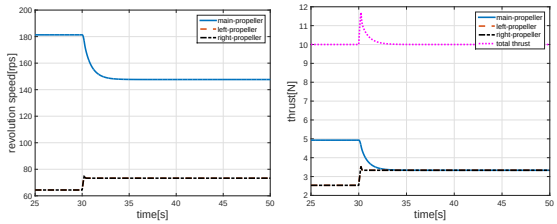

(c) Revolution speed of each propeller. (d) Thrust of each propeller.

Fig. 9. Simulation results of lift and thrust control system for step lift input.

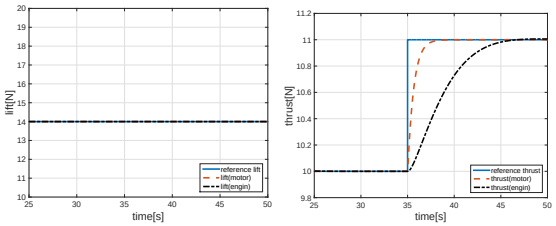

(a) Response of lift. (b) Response of thrust.

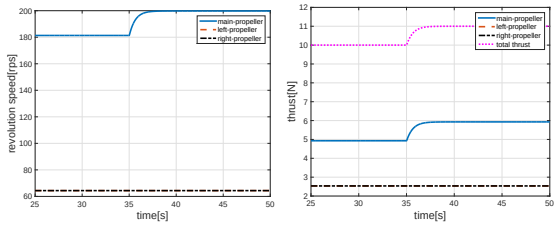

(c) Revolution speed of each propeller. (d) Thrust of each propeller.

Fig. 10. Simulation results of lift and thrust control system for step thrust input.

verified.

5. Conclusion

This paper proposed a vertical and longitudinal force concurrency control system using propeller slipstream. In this paper, the MIMO system has been built. Further more the experiment has been carried out to decide whether that the lift caused by the main-propeller revolution can be neglected. According to the experimental result, the lift caused by the main-propeller revolution can be neglected. Com-

paring the lift caused by the main-propeller revolution and the lift caused by sub-propeller, it is found that the interference between the main-propeller revolution and lift is small enough. The interference between main-propeller revolution and the lift can be neglected. Then, the simulation of proposed method has been done and compared to that of engines. The effectiveness of the proposed method is verified by simulations.

Acknowledgement

I thank Prof. Suzuki for permission to use wind tunnel. Without his guidance and persistent help this paper would not have been possible.

This research was partly supported by the Ministry of Education, Culture, Sports, Science, and Technology grant (Basic Research A, number: 26249061).

References

(1) D. Sigler:“Motor and Controller Technology”,CAFE Foundation Electric Aircraft Symposium.

(2) Y. Hori:“Future Vehicle Driven by Electricity and Control-research on Four-Wheel-Motored UOT Electric March II,”IEEE Trans. Inc. Electron, Vol. 51, No. 5, pp. 954–962, (2004)

(3) Tine Tomazic Pipistrel Taurus G4: on Creation and Evolution of the Winnig Aeroplane of NASA Green Flight Challenge 2011, INVITED PAPER. http://www.sv-jme.eu/data/upload/2011/12/02_2011_212_Tomszic_04.pdf[retrieved 16 May 2015]

(4) A.Nishizawa, H.Kobayashi, K.Okai, and H. Fujimoto:“Progress of Evolution of Electric Vehicle Technorogy and Future of Electric Aircraft,” the 43rd JSASS Annual Meeting, pp. 521–526, (2012).

(5) K. Takahashi, H. Fujimoto, Y. Hori, H. Kobayashi, and A. Nishizawa: “Airspeed Control of Electric Airplane Based on 2-Quadrant Thrust Control and Verification with Towing Test Using Electric Vehicle,” The 40th Annual Conference of the IEEE Industrial Electronics Society, (2014)

(6) N. Konishi, H. Fujimoto, Y. Watanabe, K. Suzuki, H. Kobayashi, and A. Nishizawa, : “Lift Control of Electric Airplanes by Using Propeller Slipstream for Safe Landing,” The IEEE/IES International Conference on Mechatronics, March, (2015).

(7) W. Khan and M. Nahon: “Improvement and Validation of a Propeller Slipstream Model for Small Unmanned Aerial Vehicles,” 2014 International Conference on Unmanned Aircraft Systems, May 27–30, (2014).

(8) N. Beck, R. Radespiel, C. Lenfers, J. Friedrichs, and A. Rezaeian: “Aerodynamic Effects of Propeller Slipstream on a Wing with Circulation Control,” Journal of Aircraft, Vol. 52, No. 5, September–October, (2015).

(9) M. Drela : “QPROP Formulation,” (2006) , http://web.mit.edu/drela/Public/web/qprop/qprop_theory.pdf [retrieved 1st Nov. 2015]

(10) Timmer, W. A. : “Aerodynamic Characteristics of Wind Turbine Blade Airfoils at High Angles-of-Attack,” Proceedings of TORQUE 2010: The Science of Making Torque from Wind, Crete, pp. 7178, (2010).

(11) M. Â. R. Silvestre, J. Morgado, and J. C. Páscoa: “JBLADE:a Propeller Design and Analysis Code,” 2013 International Powerd Lift Conference, AIAA paper 2013–4220, (2013).

(12) D. Marten, J. Wendler, G. Pechlivanoglou, C. N. Nayeri , and C. O. Paschereit: “QBLADE: An Open Source Tool for Design and Simulation of Horizontal and Vertical Axis Wind Turbines” *International Journal of Emerging Technology and Advanced Engineering* Vol. 3, No. 3, pp. 264–269, , Feb. (2013).

(13) J. Morgado, M. Â. R. Silvestre, and J. C. Páscoa: “Validation of Formulations for Propeller Analysis,” *Journal of Propulsion and Power*, Vol. 31, No. 1, Jan. –Feb. , pp. 467–477, (2015).

(14) G. Ananda : “UIUC propeller Database [database],” Aerospace Engineering, Univ. of Illinois Champaign, IL, http://m-selig.ae.illinois.edu/props/propDB.html [retrieved 16 Nov. 2015]

(15) APC PROPELLERS: https://www.apcprop.com/v/PERFILES_WEB/listDatafiles.asp [retrieved 5 Feb. 2015]

(16) MathWorks documentation: http://jp.mathworks.com/help/simulink/examples/engine-timing-model-with-closed-loop-control.html [retrieved 5 Feb. 2015]